AIAA JOURNAL
Vol. 32, No. 7, July 1994

Elliptic Tip Effects on the Vortex Wake of an Axisymmetric Body at Incidence

David H. Bridges*
Mississippi State University, Mississippi State, Mississippi 39762
and
Hans G. Hornung†
California Institute of Technology, Pasadena, California

The effectiveness of a new version of an elliptic cross-section tip in controlling the asymmetry of the vortex wake of an axisymmetric body at angle of attack has been studied. The elliptic cross sections were generated using two sixth-degree polynomials such that the tip radius, slope, and curvature would match those of a right circular cone at the point where the polynomial became tangent to a cone generator. The tip was found to be effective in varying the vortex wake geometry of a right circular cone at large angle of attack. The measured side force coefficient varied smoothly with tip roll angle for the two lowest angles of attack studied and exhibited square-wave and more undesirable variations for the larger angles of attack studied. These square-wave and peak, reduction-in-magnitude, and change-in-sign variations were caused by vortex breakaway, which allowed vortex crossover to occur. Ahead of vortex breakaway, the elliptic cross-section tip yielded smooth variations of vortex wake asymmetry with tip roll angle, indicating that the tip would possibly be a feasible control device for high-performance fighter aircraft at high angle of attack.

Introduction

THE problem of the side force on an axisymmetric body has been studied extensively over the last 40 years. In recent years, a number of survey papers have appeared, with those by Ericsson and Reding[1,2] and by Hunt[3] among the most complete and illuminating in that number. The reason for the great interest in this problem has been its bearing on the control of missiles and high-performance fighter aircraft at high angle of attack. If the symmetric vortex wake behind the nose of either body suddenly becomes asymmetric, a large side force can be generated on the nose, creating a large yawing moment that can result in loss of control of the missile or aircraft. In these cases, prevention of the wake asymmetry would be desirable. Alternatively, when an aircraft is at high angle of attack, the rudder is submerged in the wake of the wing and fuselage, and so its effectiveness is reduced. If a means of controlling the side force on the nose of the aircraft could be found, this force could be used to create a controllable aircraft yawing moment, and so a supplementary yaw control mechanism for aircraft at high angle of attack would be available. A desirable feature of such a mechanism would be a smooth variation in side force (and thus yawing moment) with the control parameter. A number of different side force control devices have been investigated. The two predominant methods studied have been controllable strakes and jet blowing. The works of Rao et al.,[4] Guyton et al.,[5] and Malcolm and Ng[6] are representative of these studies. The success of these attempts has been mixed. The method employed is usually able to set predictably the sign of the side force but is less successful at providing a smooth variation of side force with control parameter, whether the parameter is strake-deflection angle or jet-blowing rate. Recently, Williams and Bernhardt[7] have obtained a continuous variation of side force coefficient with jet suction ratio for a limited range of Reynolds number.

Presented as Paper 93-2960 at the AIAA 24th Fluid Dynamics Conference, Orlando, FL, July 6–9, 1993; received Sept. 25, 1993; revision received Jan. 27, 1994; accepted for publication Jan. 28, 1994.

*Assistant Professor, Department of Aerospace Engineering, P.O. Drawer A. Member AIAA.

†Clarence L. Johnson Professor of Aeronautics, Department of Aeronautics, Mail Code 105-50. Member AIAA.

Tip Asymmetry Effects

One of the most significant discoveries in the study of the side force problem has been the determination of the extreme sensitivity of the entire vortex wake to conditions at the tip of the axisymmetric body and, in particular, how microasymmetries at the tip of a nominally axisymmetric body can cause large variations in wake geometry and body side force as the body is rotated about its axis. Such discoveries have led researchers to study the effects of various controlled asymmetries at the tips of axisymmetric bodies. Moskovitz[8] and Moskovitz et al.[9] added beads to the tips of axisymmetric models; Zilliac et al.,[10] chisel tips and transverse wires. These investigators studied the variation of body side force with roll angle for the different tip geometries and obtained similar results to those found for strakes and jets in that the sign of the side force could be set predictably but not the magnitude. For these tip geometries, the side force coefficient was found to vary with body roll angle roughly as a two-cycle square wave, with large, abrupt changes in magnitude and sign as the body rotated through symmetric body/flow conditions.

Elliptic Cross Section Tips: Previous Studies

Elliptic cross section noses have already been used on aircraft to reduce the side force and yawing moment associated with the asymmetric wake of the aircraft nose. Skow and Erickson[11] summarize several investigations, particularly the work by Northrop on the F-5F "Shark" nose (described in detail by Edwards[12]), which showed that modifying the nose shape from a circular cross section to a flatter cross section yielded a significant improvement in the directional stability of the aircraft. Some of these nose cross sections, including the Shark nose on the F-5F, were elliptic.

The first to attempt the use of an elliptic cross-section tip to *control* the side force on an axisymmetric body at angle of attack was Moskovitz[8] (see also Moskovitz et al.[13]). After studying various published data, Moskovitz concluded that the flowfield asymmetry variation with body roll angle could be divided into two parts: a regular variation caused by the body being out of round, and irregular variations caused by surface imperfections. Further, he reasoned that a body with elliptic cross sections would produce a side force that would vary smoothly with body roll angle and would undergo four changes in sign over one complete revolution; i.e., the side force variation with body roll angle would be a smooth two-cycle sinusoid. To validate his hypotheses, Moskovitz constructed tips with cross sections that were elliptic near the pointed end of

the tip and that gradually became circular near the base of the tip, where the tip attached to the nose of the axisymmetric body. These tips were tested on axisymmetric bodies with conical and ogive noses. At an angle of attack of 30 deg, Moskovitz obtained smooth two-cycle sinusoids for the variation of sectional side force coefficient with roll angle for both conical and ogive noses, as expected. For angles of attack of 40 and 50 deg, the variation of sectional side force coefficient with roll angle for the body with the ogive nose was also a mostly smooth, two-cycle sinusoid. However, for the body with a conical nose and elliptic cross-section tip at angles of attack of 40 and 50 deg, Moskovitz obtained side force coefficients that varied with roll angle as a two-cycle square wave. These results were similar to those obtained with the bead, chisel, and transverse wire tip geometries discussed earlier.

This similarity in the results for the bead, chisel, and transverse wire tip geometries and Moskovitz's elliptic cross-section tip on a conical nose led the current authors to conclude that the effects of *slight* tip asymmetry had not been isolated in the tests by Moskovitz. This conclusion was reinforced by an examination of photographs of the elliptic cross-section tips in the thesis by Moskovitz,[8] which illustrated the somewhat crude nature of the tips. The authors decided to design and construct an elliptic cross-section tip that gradually and smoothly merged from elliptic to circular cross sections. The axisymmetric body to which this tip was designed to be attached was a right circular cone with a 5 deg semi-angle θ_c. The resulting tip shape is shown in Fig. 1. The major and minor axes of the elliptic cross sections were obtained from sixth-degree polynomials for axial body distance as a function of body radius. These polynomials were chosen so that tip and cone radii, slopes, and curvatures could be matched at the point where each tip polynomial became tangent to a cone generator. By choosing two different axial locations for tangency, two different polynomials could be constructed with different radii of curvature near the origin and hence different "widths" near the origin. The representative length scale for the tip was chosen to be the geometric mean of the radii of curvature of the two polynomials at the origin, denoted by R_t. For this tip, R_t was 0.942 cm. The details of the design and construction of this tip may be found in the thesis by Bridges.[14]

The results of preliminary investigations with this tip were reported in a previous paper by the authors.[15] These results indicated

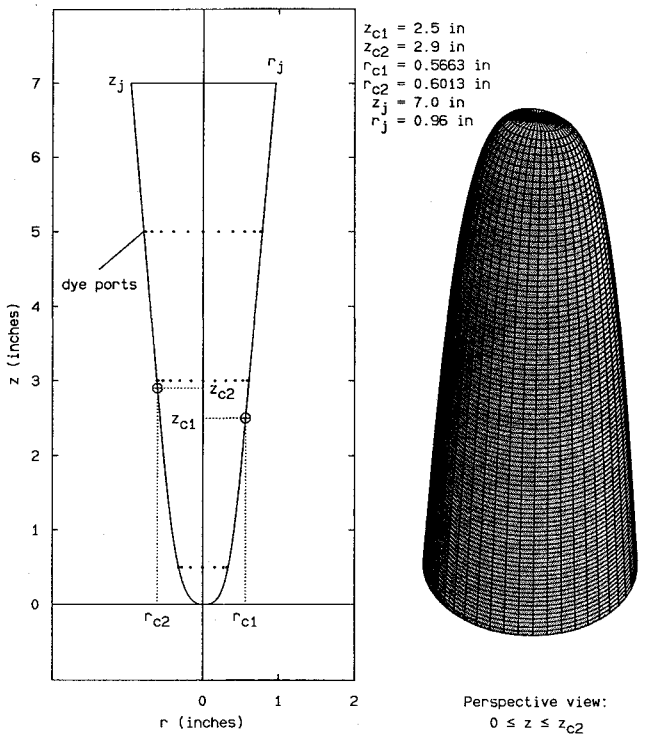

Fig. 1 Elliptic cross-section tip.

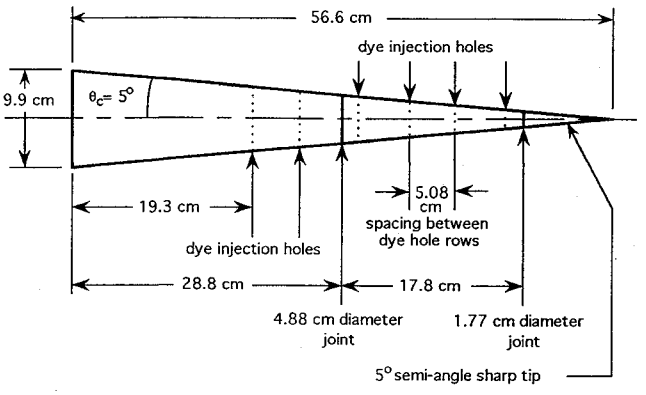

Fig. 2 Cone model.

that the tip could provide smooth variation of vortex wake asymmetry with variation of the control parameter, in this case the tip roll angle ϕ, for a body with a conical nose and at an angle of attack at which the tip by Moskovitz, on a body with a conical nose, had produced square-wave variations of side force coefficient with roll angle. To establish the effectiveness of this tip in controlling body side force, the authors knew that the actual side force variations with tip roll angle for this tip/body combination would have to be measured for a larger range of Reynolds numbers. Thus a set of force measurement experiments was planned and conducted. The results of these experiments were somewhat unexpected, leading to a more extensive set of flow visualization experiments to understand what was happening in the vortex wake.

Force Measurements

Experimental Apparatus and Procedure

The force measurement experiments were conducted using the elliptic cross section tip described earlier. The cone to which the tip was attached is shown in Fig. 2. The cone had a 5-deg semi-angle θ_c and a base diameter D of 9.9 cm. Both the cone and tip were constructed with holes so that dye could be injected into the flow from within the model. The elliptic cross-section tip was constructed to be attached to the cone at the 4.88 cm threaded joint. The overall length of the cone and tip combination was 46.6 cm or 4.7D. The cone was attached to a sting mechanism such that the angle of attack α of the cone could be set between 0 and 100 deg in 10-deg increments. The sting also included a stepper motor that was used to rotate the cone about its axis and a rotary optical encoder to insure that commanded rotations were executed. The cone and sting mechanism were suspended from a Task Corporation 2.00 Mk II six-component strain-gauge force balance. A Scientific Solutions 12-bit analog-to-digital converter was used to sample the signals from the balance amplifier system.

The facility used in these experiments was the Free Surface Water Tunnel (FSWT) of the Hydrodynamics Laboratory at the California Institute of Technology. The test section of the FSWT was 50.8 cm wide, 50.8 cm high, and 2 m long. The speed range used in these experiments was 0.3 m/s < U_∞ < 0.9 m/s. The reported freestream turbulence level in this facility was 0.38% at a freestream speed of 4.6 m/s (see the article by Ward[16] for further details regarding this facility).

Once the sting was attached to the elevating mechanism, the cone was attached to the sting at $\alpha = 0$ deg, and the zero roll angle ϕ_o was measured to an accuracy of ± 0.1 deg. Zero roll angle corresponded to the major axes of the elliptic cross sections being vertical when viewed from the base of the model. Increasing ϕ corresponded to a clockwise rotation when viewed from the base of the cone. The angle of attack α was then set and measured with a digital inclinometer with an accuracy of ± 0.1 deg. In this configuration, the force balance measured the forces on the entire tip-cone model plus whatever portion of the sting that happened to be submerged (i.e., this model had no metric and nonmetric portions). The sideslip angle β was set to zero with an accuracy of ± 0.1 deg. A surface plate was used to reduce free surface effects. Once the

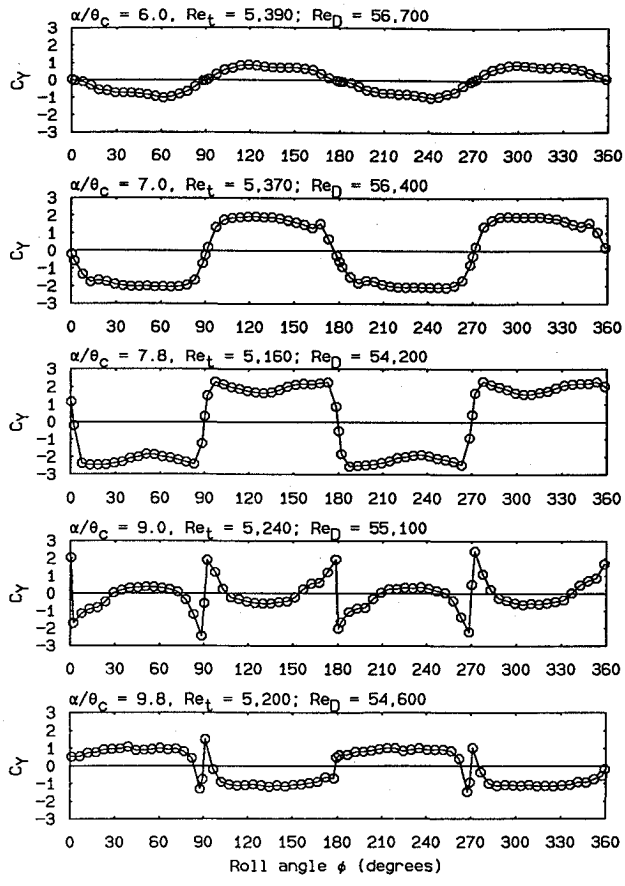

Fig. 3 Angle of attack effects: nominal U_∞ = 0.5 m/s.

cone was put into position, the outputs of the force balance bridges were set to zero, permitting the measurement of fluid dynamic forces alone, without having to consider the loads at zero speed caused by the model weight. During each roll angle sweep, a Gateway 2000 386-20 computer stepped the cone to a particular roll angle and then read the output of the optical encoder to confirm the step. After the step, the computer delayed for four axial flow periods (the model length divided by the axial component of the freestream velocity, $U_\infty \cos \alpha$). After the delay, the computer sampled the balance output voltages 100 times, the samples being evenly spaced over four axial flow periods, and computed the average and rms values of the voltages. Then, the cone was stepped to the next roll angle and the process repeated until the roll angle sweep was completed.

Side forces were measured on the tip/cone model for nominal angles of attack of 30, 35, 40, 45, 50, and 60 deg, corresponding to nominal α/θ_c values of 6, 7, 8, 9, 10, and 12, respectively, and at nominal freestream speeds of 0.3, 0.5, 0.7, and 0.9 m/s, corresponding to nominal tip Reynolds number values of 2.8×10^3, 4.7×10^3, 6.6×10^3, and 8.5×10^3, and to nominal base diameter Reynolds number values of 2.97×10^4, 4.95×10^4, 6.93×10^4, and 8.91×10^4, respectively. The side forces were measured and converted into side force coefficients C_Y using the freestream dynamic pressure and the cone base area $\pi D^2/4$. The bounds on the test section blockage estimated for this model were a minimum of 5% and a maximum of 9.3%. Because of the small difference in the limits of the blockage, no blockage corrections were applied to the data.

Results

The variations of side force coefficient with roll angle for a nominal freestream speed of 0.5 m/s and all values of α/θ_c are shown in Fig. 3. The results for only one nominal speed are shown because of the lack of Reynolds number effects on the variation of C_Y with ϕ, which is shown in Fig. 4 for α = 39 deg (α/θ_c = 7.8), and which was typical of all of the side force measurements conducted in this study. This was to be expected. The primary viscous effect in flows past bodies at large angle of attack is the circumferential location of the boundary-layer separation points. For laminar separations, these separation locations are essentially independent of Reynolds number. The largest base diameter Reynolds number Re_D studied in the current experiments was approximately 1.0×10^5, implying that all of the separations in these experiments were laminar, according to the laminar/transitional separation boundary established by Lamont.[17] Therefore, the circumferential separation points were fixed so that no Reynolds number effects should be expected. For this reason, the variations of C_Y with ϕ at a nominal freestream speed of 0.5 m/s shown in Fig. 3 are representative of all of the side force measurement results.

Unfortunately, the representative results shown in Fig. 3 were not the expected results. At α/θ_c = 6.0, the variation of C_Y with ϕ was an approximately smooth, two-cycle sinusoid, as expected. At α/θ_c = 7.0, the variation continued to be smooth, although a squaring of the C_Y-ϕ characteristic began to appear. At α/θ_c = 7.8, the variation of C_Y with ϕ became a two-cycle square wave similar to that observed by the investigators mentioned previously. For α/θ_c = 9.0 and 9.8, the results were even more undesirable. Not only were there large, rapid changes in C_Y as ϕ passed through one of the two symmetry conditions, with peaks on either side of the zero crossings, but between those peak values, C_Y decreased in value and even changed sign, as shown for α/θ_c = 9.8. In particular, note for example that for 90 deg < ϕ < 180 deg, the sign of C_Y at α/θ_c = 9.8 is opposite to that at α/θ_c = 7.0. In the area of aircraft stability and control, this would be referred to as control reversal.

A number of tests were conducted to insure the reliability of the data. Roll hysteresis checks indicated that the C_Y-ϕ characteristics had no dependence on the direction of the roll angle sweep. Speed hysteresis checks yielded a similar result. These tests also confirmed the repeatability of the data. End effect tests showed that only the magnitudes and not the shapes of the C_Y-ϕ characteristics were affected by end conditions.

Flow Visualization Experiments

Introduction

As stated before, the results obtained for the variation of side force coefficient with tip roll angle were not the expected results. The smooth variation of vortex wake asymmetry with tip roll angle observed in the preliminary experiments did not translate into a smooth variation of side force coefficient, at least at the larger angles of attack where such a variation was most desirable. A more extensive set of flow visualization experiments was conducted to determine the reasons for the unexpected behavior. These experiments measured the changes in vortex positions as the cone was rotated about its axis for various angles of attack and speeds.

Estimated Side Force Calculation

To obtain an idea of how changes in the vortex wake geometry might affect the side force on the cone, the side force on a circular

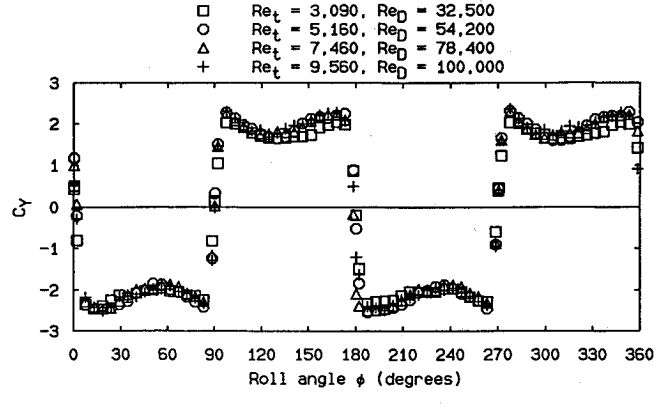

Fig. 4 Reynolds number independence: α/θ_c = 7.8.

cylinder in potential flow with two vortices of arbitrary strengths placed at arbitrary locations behind the cylinder was calculated. The resulting sectional side force was then integrated over the cone to give the side force on the body. The vortex locations measured from the experiments and an estimate of the vortex strengths were used in the resulting formula for side force coefficient.

The complex potential for the flow past a circular cylinder of radius a placed at the origin in a crossflow of velocity U and with two vortices with strengths Γ_1 and Γ_2 placed at $z_1 = (x_1, iy_1)$ and $z_2 = (x_2, iy_2)$, respectively, is given by

$$W = U\left(z + \frac{a^2}{z}\right) + \frac{i\Gamma_1}{2\pi}\left[-\log(z - z_1) + \log\left(z - \frac{a^2}{z_1^*}\right) - \log z\right]$$

$$+ \frac{i\Gamma_2}{2\pi}\left[-\log(z - z_2) + \log\left(z - \frac{a^2}{z_2^*}\right) - \log z\right] \tag{1}$$

where $i = (-1)^{1/2}$, $z = x + iy$, $z_j = x_j + iy_j$, $j = 1, 2$, and z_1^* and z_2^* are the complex conjugates of z_1 and z_2, respectively. Using the Blasius formula for the forces on a body in a potential flowfield,

$$X - iY = \frac{i\rho}{2}\oint_C \left(\frac{dW}{dz}\right)^2 dz \tag{2}$$

choosing for the contour of integration C the body contour given by $z = ae^{i\theta}$, $0 \le \theta \le 2\pi$, integrating using Eq. (2), and then nondimensionalizing the coordinates by a, the vortex strengths by $2\pi aU$, and the forces by $\rho U^2 a/2$, the following result is obtained for the nondimensional sectional side force coefficients C_x and C_y:

$$\frac{1}{4\pi}(C_x - iC_y) = \frac{i\gamma_1}{z_1^2} + \frac{i\gamma_2}{z_2^2} + \gamma_1^2\frac{z_1^*}{z_1 z_1^* - 1} + \gamma_2^2\frac{z_2^*}{z_2 z_2^* - 1}$$

$$-(\gamma_1\gamma_2 + \gamma_1^2)\frac{1}{z_1} - (\gamma_1\gamma_2 + \gamma_2^2)\frac{1}{z_2} - \gamma_1\gamma_2\left(\frac{z_1^*}{1 - z_2 z_1^*} + \frac{z_2^*}{1 - z_1 z_2^*}\right) \tag{3}$$

where z, z_1, z_1^*, z_2, and z_2^* are now used to denote *nondimensional* values, and γ_1 and γ_2 are the nondimensional vortex strengths. If conical flow past a conical body is assumed, then the dimensionless vortex coordinates z_1 and z_2 are independent of the axial body coordinate. If in addition the dimensionless vortex strengths are assumed to be constant, which implies that the actual vortex strengths Γ_j grow linearly with the axial body coordinate Z in the form $\Gamma_j = 2\pi U\gamma_j Z \tan\theta_c$, $j = 1, 2$, then the result for the sectional force coefficients given by Eq. (3) is independent of the axial coordinate Z. Assuming both conical flow and a completely conical body, integrating Eq. (3) along the cone gives the following relationship between the sectional body side force coefficient obtained from (3) and the total body side force coefficient:

$$C_Y = \frac{Y}{(1/2)\rho U_\infty^2(\pi D^2/4)} = \frac{\sin^2\alpha}{2\pi\tan\theta_c}C_y \tag{4}$$

Equation (3) requires the positions and strengths of the two wake vortices. The experiments gave the vortex positions but no information about their strengths. Thus some sort of estimate for the vortex strengths was required. Previous investigations[18,19] have shown that, in general, the vortex closer to the body is stronger than the vortex farther away. This trend was incorporated into a model of the vortex strength as a function of the dimensionless radial distance r/a from the centerline of the cone. This model is shown in Fig. 5. The model consisted of two parts: a linear variation of vortex strength with radial distance and then an inverse power law variation, used so that the vortex strength would continue to decrease with increasing radial distance without changing

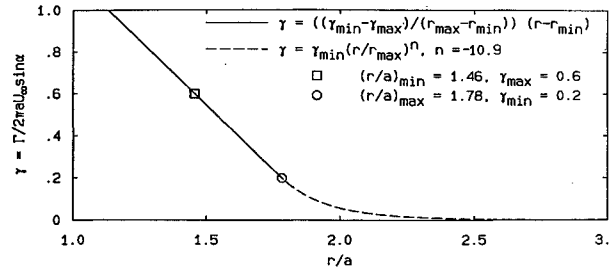

Fig. 5 Nondimensional vortex strength model.

sign. The endpoints of the linear portion of the curve were chosen by adjusting maximum and minimum values of vortex strength assigned to minimum and maximum measured vortex radial distances, respectively, until the computed side force coefficients using the measured vortex locations for a particular angle of attack matched the measured C_Y values at that angle of attack. The exponent n for the power-law portion was then chosen so that the slopes of the two segments of the curve would match at $(r/a)_{max}$. The angle of attack chosen was 30 deg ($\alpha/\theta_c = 6$) because at this angle of attack the measured side force coefficients had the smoothest variation with tip roll angle. This model was then used for all other angles of attack. The model did better at predicting trends in side force variations than in actual magnitudes for higher angles of attack, and so in all of the results to be presented, the computed side force coefficients were scaled so that the peak computed and measured C_Y values for a particular test had the same magnitude. A number of assumptions and approximations went into these calculations of side force coefficient. However, the main purpose of the calculations was to get an idea of how changes in the vortex wake *geometry* might change the body side force, and for that purpose, the model was deemed sufficient. For more details concerning the construction of the vortex wake model, see the thesis by Bridges.[14]

Apparatus and Procedure

The model was tested in a low-speed, free-surface water channel with a freestream turbulence level on the order of 0.1% (details concerning this facility may be found in Refs. 14 and 15). The experimental apparatus used is shown in Fig. 6. In this figure, the laser and optics used to create the laser sheet have been omitted. Fluorescein dye was injected from within the model and illuminated with a laser sheet aligned perpendicular to both the model axis and the incidence plane (the plane defined by the body axis and the freestream velocity vector), producing a cross section of the vortex wake. The image of the vortex wake cross section was reflected in a mirror suspended vertically in the model wake and mounted at a 45 deg angle to the incidence plane. The mirror was 1.8 cone base diameters D high and $1.5D$ wide and was located at least $5D$ downstream of the base of the cone. The mirror could be aligned with an estimated accuracy of ± 1 deg. The image was recorded by the video camera and then digitized using image processing software. The distortion caused by the off-axis view of the cross section was removed by fitting the equation of an ellipse to points on the sheet-cone intersection line. By normalizing the abscissa of the vortex location with the ellipse major axis and the ordinate with the minor axis, the distortion was removed, and the vortex coordinates, normalized by the local radius of the cone (the radius at which the sheet intersected the cone), were found. The estimated error in the resulting vortex locations was between 5 and 10%. However, since the goal of these experiments was primarily to investigate qualitative vortex wake variations with tip roll angle as speed and angle of attack were varied, the data were deemed sufficiently accurate for the purposes of the investigation.

Variations of vortex wake geometry with tip roll angle were studied for three angles of attack, 30, 40, and 45 deg, corresponding to $\alpha/\theta_c = 6$, 8, and 9, respectively. The three speeds tested, 0.1, 0.15, and 0.2 m/s, corresponded to tip Reynolds numbers Re_t of 9.42×10^2, 1.413×10^3, and 1.884×10^3, and to base diameter

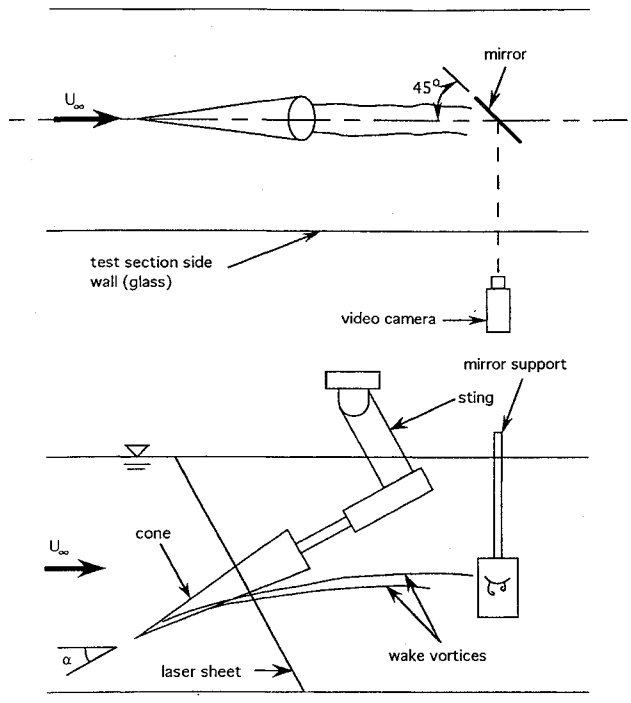

Fig. 6 Apparatus for flow visualization experiments.

Reynolds numbers Re_D of 9.9×10^3, 1.485×10^4, and 1.98×10^4, respectively. Because of the number of cases to be studied and the large amount of time required for data reduction for each case, only partial roll angle sweeps of $45 \le \phi \le 135$ deg were conducted for some flow conditions. The endpoints of the partial roll angle sweeps corresponded to the maximum body/flow asymmetry conditions on either side of the symmetric body/flow condition in which the plane formed by the major axes of the elliptic cross sections was perpendicular to the incidence plane. These roll-angle-sweep endpoints are illustrated in Fig. 7 for purposes of orientation.

Results

The basic results for the vortex wake geometry experiments are shown in Figs. 8–12. Each figure contains the measured vortex positions made dimensionless by the radius of the cone R_c at the location of the laser sheet and a comparison of the measured and calculated side force coefficients at each angle of attack and laser sheet location. The angle of attack is nondimensionalized by the cone semi-angle θ_c, and the laser sheet location Z_{ls} is nondimensionalized by the total length L of the model and tip. The Föppl potential flow solution for two stationary vortices behind a circular cylinder[20] is included for comparison purposes.

The most significant result shown in these figures is the change in the behavior of the wake geometry between the fore and aft laser sheet locations for the two highest angles of attack. Figure 8 shows that at $\alpha = 30$ deg ($\alpha/\theta_c = 6$) and a laser sheet location $Z_{ls}/L = 0.59$, the aftmost laser sheet location used in these studies, the variation of vortex location with tip roll angle was small, and the calculated C_Y demonstrated the smooth sinusoidal variation with ϕ shown by the measured side coefficients. For angles of attack of 40 deg ($\alpha/\theta_c = 8$) and 45 deg ($\alpha/\theta_c = 9$) and the forward laser sheet location ($Z_{ls}/L = 0.28$), the variation in measured vortex location with roll angle shown by Figs. 9 and 11 is also small, but the corresponding smooth variation in calculated side force coefficient is in contrast to the square-wave behavior of the measured side force coefficients at $\alpha = 40$ deg (Fig. 9) and the peak, reduction-in-magnitude, and change-in-sign behavior of the measured C_Y at $\alpha = 45$ deg (Fig. 11). However, at $\alpha = 40$ deg and an aft laser sheet location $Z_{ls}/L = 0.48$, Fig. 10 shows that the measured vortex locations had a much larger variation with tip roll angle, and the side force coefficients computed from these locations began to imitate the square-wave behavior of the measured side force coefficients. At $\alpha = 45$ deg and an aft laser sheet location $Z_{ls}/L = 0.48$, Fig. 12 shows that the measured vortex locations had an even larger variation with tip roll angle, and the side force coefficients calculated from these locations began to imitate the peak, reduction-in-magnitude, and change-in-sign behavior of the measured side force coefficients. These matches in behavior of the side force coefficient, and the recognition that sectional pressure distributions toward the rear of the cone would have a larger contribution to the overall side force than such distributions near the tip, would indicate that the measured variations in vortex wake geometry were sufficient to explain the unexpected and undesired C_Y behavior for the larger angles of attack.

The main difference between the wake geometry results for the fore and aft laser sheet locations is the position of the vortex in each pair of vortices that is closer to the cone. For the smaller Z_{ls}/L, each vortex in each pair of vortices remains to one side of the cone centerline. However, for the larger Z_{ls}/L, after the vortex pair passes through the symmetric wake configuration, the vortex that is closer to the cone sometimes actually crosses to the opposite side of the cone centerline. This can be seen for a few vortex loca-

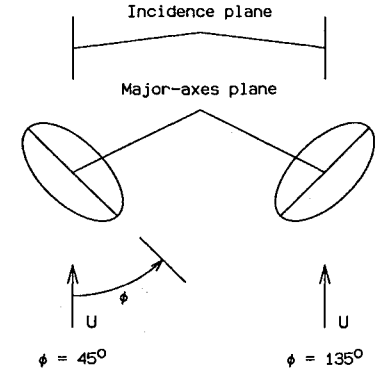

Fig. 7 Endpoints for partial ϕ sweeps.

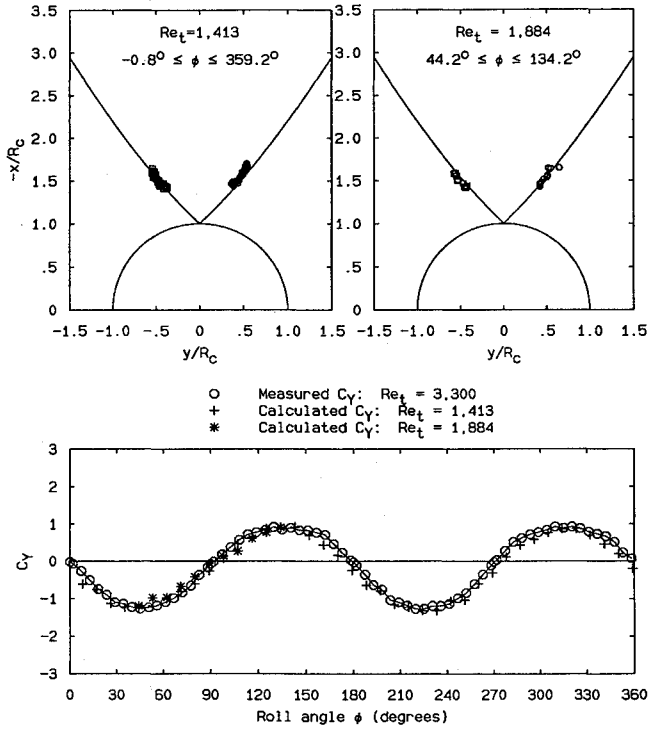

Fig. 8 Vortex wake geometry: $\alpha/\theta_c = 6$ and $Z_{ls}/L = 0.59$.

tions in Fig. 10, where $\alpha = 40$ deg ($\alpha/\theta_c = 8$) and $Z_{ls}/L = 0.48$. The most dramatic evidence of "vortex crossover" is shown in Fig. 12, where $\alpha = 45$ deg ($\alpha/\theta_c = 9$) and $Z_{ls}/L = 0.48$. Note that the squares in this figure correspond to the left vortex in the vortex pair, and that when the left vortex is closer to the cone than the right vortex, the *left* vortex is to the *right* of the cone centerline for the majority of such vortex positions. A similar note can be made for the right vortex in each pair, denoted by circles in the figure. This crossover is just beginning at $\alpha = 40$ deg for $Z_{ls}/L = 0.48$ (Fig. 10). At this angle of attack and laser sheet location, the variation of the computed side force coefficient is just beginning to approach the square-wave behavior of the measured C_Y. The large number of occurrences of vortex crossover at $\alpha = 45$ deg and $Z_{ls}/L = 0.48$ (Fig. 12) appear at the same time that the computed C_Y are beginning to show the peak, reduction-in-magnitude, and change-of-sign behavior of the measured side force coefficients at that angle of attack.

How this vortex wake geometry behavior could be related to the side force coefficient behavior can be understood from an examination of Fig. 13. This figure shows the vortex locations corresponding to 44.2 deg $\leq \phi \leq$ 134.2 deg at $\alpha = 45$ deg and $Re_t = 9.42 \times 10^2$. The pair of connected vortex locations labeled "ϕ = 89.5 deg" corresponds to an essentially symmetric vortex wake geometry, and the corresponding computed C_Y is almost zero. As ϕ moves away from this value to the next value on either side, ϕ = 80.5 or 98.5 deg, the vortices undergo a relatively large shift to an asymmetric configuration that results in the maximum computed C_Y. The vortex in the asymmetric pair that ends up closer to the cone was on the opposite side of the cone centerline when the vortex wake was symmetric; i.e., crossover has occurred. As ϕ moves still further away from 89.5 deg, the vortices become even more asymmetric, but the magnitude of the computed C_Y is reduced. This could be caused by the fact that the vortex closer to the body has moved sufficiently far across the centerline of the body to reduce its influence on the side of the body on which it was located when the wake was symmetric.

As discussed earlier, the vortex crossover and subsequent deviation of the computed side force coefficients from a smooth variation with roll angle occurred at the aft laser sheet locations. To determine the axial location at which such behavior might appear, two axial traverses of the vortex wake were conducted: one at $\alpha =$ 40 deg ($\alpha/\theta_c = 8$) and $Re_t = 1.884 \times 10^3$, and one at $\alpha = 45$ deg ($\alpha/\theta_c = 9$), and both at $\phi = 44.2$ deg, corresponding to a condition of maximum body/flow asymmetry (see Fig. 7). The results of these traverses are shown in Figs. 14 and 15. Note that the origin for Z_{ls} is the origin of the elliptic cross-section tip. Figure 14 shows that the vortex crossover seems to have begun at $Z_{ls}/L \approx 0.48$ for $\alpha/\theta_c =$ 8 and $\phi = 44.2$ deg, and that the magnitude of the crossover was not large for any Z_{ls}/L at which measurements were made. However, Fig. 15 shows that, for $\alpha/\theta_c = 9$, the crossover began earlier, at $Z_{ls}/L \approx 0.34$, and that the degree of crossover seems to be in-

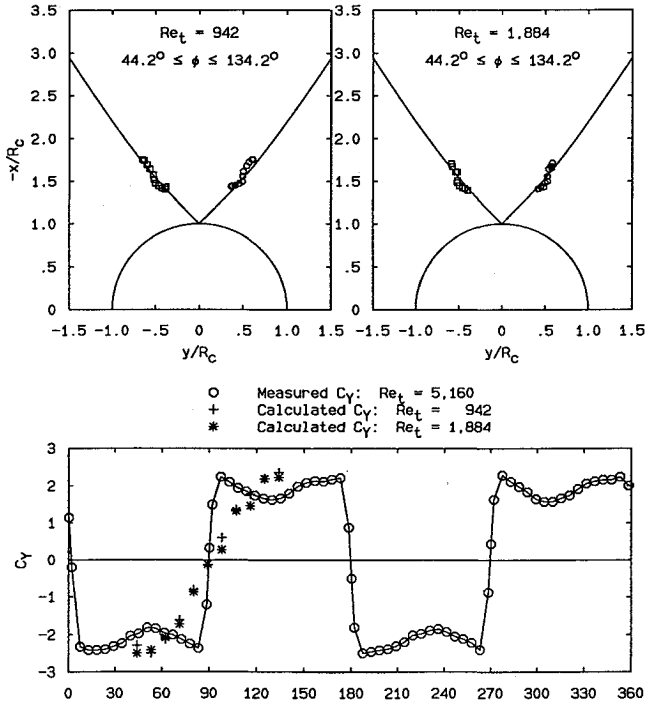

Fig. 9 Vortex wake geometry: $\alpha/\theta_c = 8$ and $Z_{ls}/L = 0.28$.

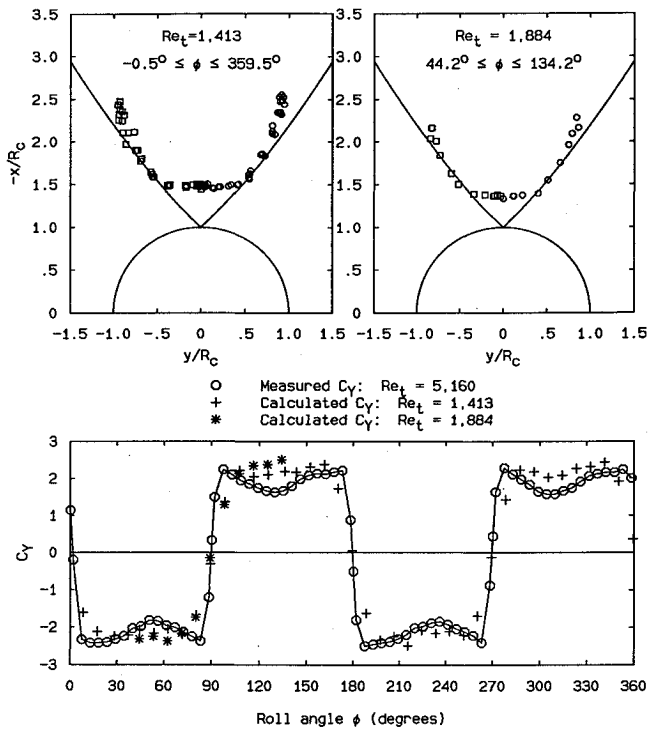

Fig. 10 Vortex wake geometry: $\alpha/\theta_c = 8$ and $Z_{ls}/L = 0.48$.

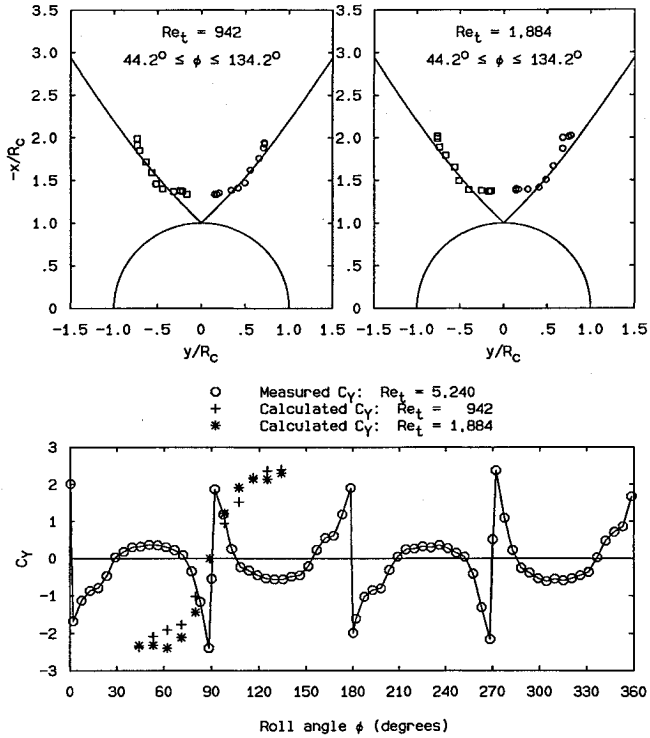

Fig. 11 Vortex wake geometry: $\alpha/\theta_c = 9$ and $Z_{ls}/L = 0.28$.

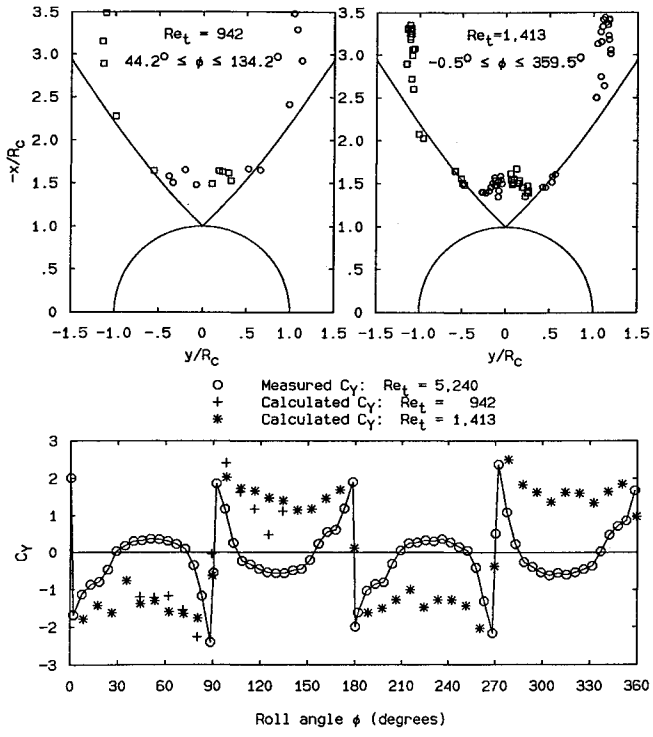

Fig. 12 Vortex wake geometry: $\alpha/\theta_c = 9$ and $Z_{ls}/L = 0.48$.

creasing slightly as Z_{ls}/L increases. In both of these cases, the crossover begins in the region where one vortex begins to break away from the cone. The motion of the one vortex away from the cone allows the other vortex to move underneath it, crossing over the centerline of the cone in the process. Recall the previous discussion that attributed the peak in the magnitude of C_Y after the zero crossing to the large shift of the vortex pair away from the symmetric configuration and then attributed the subsequent reduction in magnitude of C_Y to increasing vortex crossover that reduced the influence of the vortex closer to the body on the side of the body on which the vortex was located when the wake was symmetric. If this analysis is correct, then it is the breakaway of one vortex that leads ultimately to the reduction in magnitude of C_Y between magnitude peaks.

Such behavior has been observed by previous investigators. Ward and Katz[21] measured vortex trajectories that show a connection between vortex breakaway and vortex crossover. Wardlaw and Yanta,[19] among others, noted that the peak in the distribution of sectional side force over the length of an axisymmetric body at incidence occurred when the first vortex was shed from the body. The side force was directed away from the side of the body from which the vortex had been shed. The relation between vortex breakaway and body side force was shown explicitly by the work of Kompenhans and Hartmann,[22] who investigated the wake of an axisymmetric ogive nose of fineness ratio 3 mounted on a cylindrical afterbody at an angle of attack of 55 deg and a body diameter Reynolds number $Re_D = 2.5 \times 10^5$. The separation in this case was reported to be laminar. Kompenhans and Hartmann used a laser sheet flow visualization method similar to the one used in the current experiments to determine vortex positions and compared these positions with pressure distributions measured at the same axial locations. They discovered that, at the initial appearance of wake asymmetry, one vortex began to move away from the body and the other vortex began to move underneath the first. The pressure distributions showed a suction peak on the side of the body where the vortex closer to the body was originally located. After the near vortex crossed the body centerline, near the axial location where the far vortex could be said to have broken away from the body, the suction peak changed body sides, a change that would lead to a change in sign of the sectional side force. Kompenhans and Hartmann attributed the change of side of the suction peak to a third vortex that appeared underneath and on the same side of the body as the vortex that had broken away. Their results clearly indicated that the close vortex could not have crossed over nor could the third vortex have formed unless the far vortex had broken away. These results are all consistent with the findings of the current experiments regarding the connections between vortex breakaway and side force coefficient behavior discussed earlier.

The effects of vortex breakaway might explain why Moskovitz[8] obtained relatively smooth variations of sectional side force coefficient with roll angle for his elliptic cross-section tip on an ogive-cylinder body, and square-wave variations for his elliptic cross-section tip on a cone-cylinder body. Flow visualization photographs in the thesis by Moskovitz[8] show that, in general, for a given angle of attack, the vortices remained attached to the body for a greater axial distance on the ogive-nosed body. Moskovitz obtained sectional side force coefficients by integrating the pressure distributions obtained from pressure tap rings at identical axial locations on both noses. The photographs in the thesis taken as a whole suggest that, for a given angle of attack, vortex breakaway occurred downstream of the pressure tap rings for the ogive-nosed body and upstream of the rings for the cone-nosed body, leading to side force coefficient variations with body roll angle similar to those described earlier. One photograph does show that, for the ogive-nosed body at the largest angle of attack studied, vortex breakaway occurred upstream of the aftmost pressure tap ring. The sectional side force coefficient corresponding to this ring and this flow condition demonstrates a square-wave behavior, in contrast to the smooth variation shown at this flow condition for the two rings upstream of the vortex breakaway.

An understanding of the effects of vortex breakaway led to the question of whether or not the elliptic cross-section tip was effective in providing smooth variation of side force coefficient with roll angle ahead of vortex breakaway for large angle of attack. This question was partially answered by Figs. 9 and 11, which show a somewhat smooth variation in computed side force coefficient for $\alpha = 40$ ($\alpha/\theta_c = 8$) and 45 deg ($\alpha/\theta_c = 9$), respectively, for $Z_{ls}/L =$

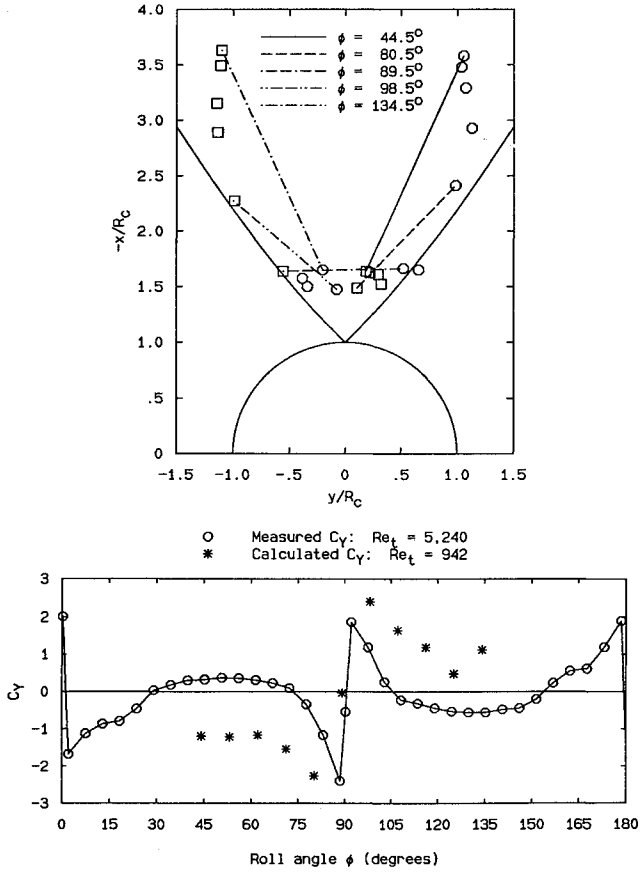

Fig. 13 Detail of wake behavior: $\alpha/\theta_c = 9$ and $Z_{ls}/L = 0.48$.

0.28. This laser sheet location is ahead of the breakaway and crossover at $\alpha = 40$ deg shown in Fig. 14, and essentially at the beginning of the breakaway and crossover at $\alpha = 45$ deg shown in Fig. 15. The ability of the tip to provide smooth variation of side force coefficient ahead of vortex breakaway at large angle of attack is shown more graphically in Fig. 16, which shows the variation of vortex position and computed side force coefficient for $\alpha = 45$ deg ($\alpha/\theta_c = 9$) for a laser sheet location $Z_{ls}/L = 0.17$, well ahead of the vortex breakaway for this angle of attack shown in Fig. 15. The variation of vortex position is small, and the variation in computed side force coefficient with roll angle is very smooth, a desirable characteristic for a control device.

It would appear, then, that it is vortex breakaway that limits the ability of a disturbance introduced at the tip of a body to control the vortex wake asymmetry. This problem is a part of the general problem of determining the particular mechanism through which conditions at the body tip affect the vortex wake further downstream. The evidence seems to indicate a traveling-wave phenomenon in which vortex wake asymmetry and breakaway are the results of perturbations that are introduced at the tip and grow as they move downstream. If this description is correct, then vortex breakaway might be explained as the result of the saturation of the vortex wake by the disturbance introduced at the tip. The traveling-wave idea was expressed in a more concrete manner by Degani and Tobak,[23] who conducted experiments that indicated that the mean asymmetric force on a body at high angle of attack is the result of a convective instability of the vortex wake, so that the wake requires the continual introduction of disturbances at the tip to maintain asymmetry.

To exploit this mechanism to control the vortex wake asymmetry, however, the response of the wake to disturbances needs to be understood more thoroughly. First, what is the effect of the size of the disturbance? Work conducted during the present study with a

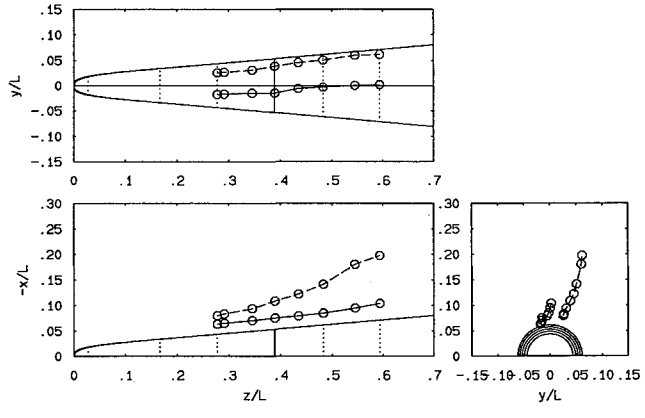

Fig. 14 Vortex trajectories: $\alpha/\theta_c = 8$, $Re_t = 1.884 \times 10^3$, and $\phi = 44.2$ deg.

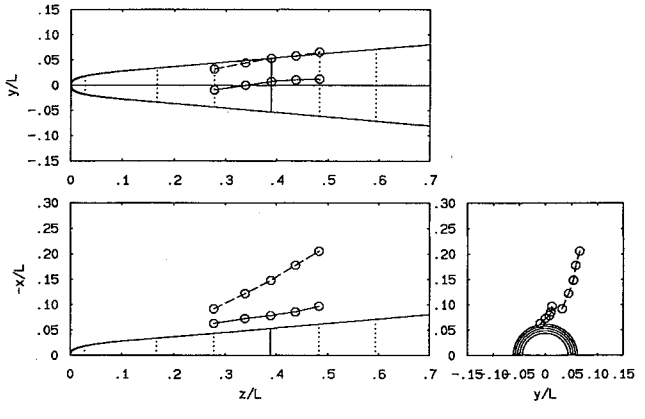

Fig. 15 Vortex trajectories: $\alpha/\theta_c = 9$, $Re_t = 942$, and $\phi = 44.2$ deg.

different, flatter elliptic cross-section tip indicated indirectly that the growth of the disturbances was a function of the initial perturbation strength: the larger the initial perturbation, the faster the growth (see Ref. 14 for details). Next, what is the response of the wake to a disturbance of a prescribed strength? Figures 9–12, which show that the variation in vortex position at a given laser sheet location increased as the angle of attack increased, indicate that the downstream growth of the disturbance introduced by the tip was greater for a higher angle of attack. Work by previous researchers[1–3] has shown that the sensitivity of the vortex wake to the perturbations introduced by the tip is set by the angle of attack through the relative angle of attack α/θ_A, where θ_A is the nose apex semi-angle. Keener and Chapman[24] have argued that the asymmetric wake is the result of a hydrodynamic instability that occurs when the two wake vortices are "crowded together" near the tip of the body. A larger nose apex angle increases the distance between the vortices and thus reduces vortex "crowding," so that a higher angle of attack is required for onset of wake asymmetry. This analysis helps to explain why, in the experiments of Moskovitz,[8] the vortices remained attached to the body with the ogive nose longer than the body with the conical nose, for a given angle of attack. For equal fineness ratios, which the two noses used by Moskovitz had, the apex angle of the ogive nose would be greater than that of the cone. The vortices behind the ogive-nosed body would be separated more and thus would be less sensitive to disturbances. Therefore the growth rate of the asymmetry would be lower and the vortices would remain attached further back on the body. Whether or not the initial wake asymmetry is the result of an inviscid instability is still in dispute, as evidenced by the article by Ericsson.[25] However, the growth of the wake asymmetry after the initial disturbance at the tip seems to be explained most readily by some sort of instability mechanism associated with the primary wake vortices, i.e., an inviscid instability. Finally, what is the saturation limit for the wake? Bernhardt and Williams have measured what they term the "distortion energy" of the asymmetric vortex wake. This square of the difference between the velocity at a particular point in an asymmetric wake and the velocity at that same point in a symmetric wake, integrated across the wake, is taken to be a measure of the distortion of the vortex wake from symmetric to asymmetric. Their measurements show that the distortion energy at first grows exponentially with increasing axial distance along the body and then levels off and is roughly constant with increasing axial distance. This leveling off is typically what occurs when a system saturates. Bernhardt and Williams report that their vortex wake "saturates" just upstream of vortex separation or breakaway. This evidence supports the idea that vortex breakaway is the result of the saturation of the vortex wake by the disturbance introduced at the tip.

Other unanswered questions remain. One of these is the effectiveness of the tip when the boundary-layer separations are transitional or turbulent. As demonstrated by Keener,[27] in the transitional regime, the asymmetric separation locations are controlled by the asymmetric transition locations so that the state of the boundary layer has an impact on the vortex wake asymmetry. If, however, the tip effectiveness is a result of the modification of the circumferential pressure distribution on the nose (i.e., an inviscid effect), then perhaps the tip effectiveness would not be diminished at a large Reynolds number, at least in the fully turbulent separation regime. This supposition needs to be verified experimentally. Another unanswered question is the effect of compressibility. Mach number effects are less significant, however, because maneuvers at high angle of attack are typically executed at subsonic Mach number.

Since the elliptic cross-section tip in the current experiments is only effective in providing smooth control of vortex wake asymmetry up to the point of vortex breakaway, it would probably not be an effective control device for a missile, since it does not prevent breakaway. However, the tip would possibly be effective in controlling the side force on the nose of an aircraft, where vortex breakaway does not usually occur before the nose ends and the fuselage begins, as illustrated by the flow visualization photographs of Chambers et al.[28] and Skow and Erickson.[11] This statement is

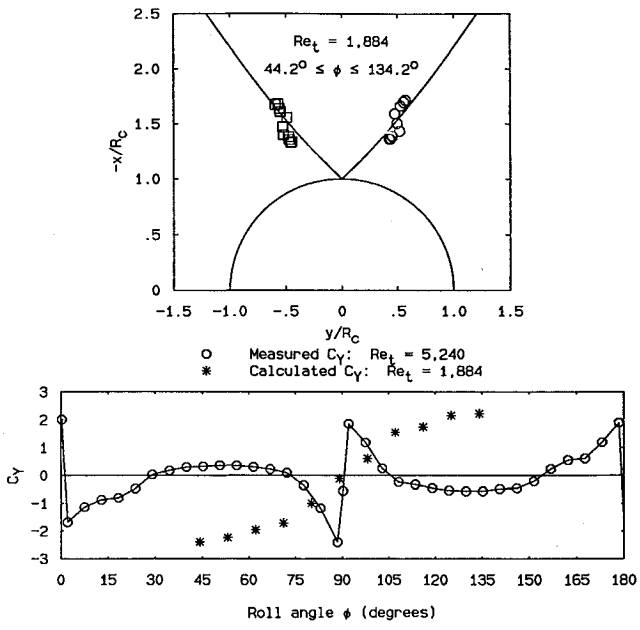

Fig. 16 Vortex wake geometry: $\alpha/\theta_c = 9$ and $Z_{ls}/L = 0.17$.

supported by Keener and Chapman,[29] who conclude that the presence of a wing tends to reduce or eliminate the influence of the afterbody on asymmetric side forces. If the elliptic cross section tip could provide a smooth variation of vortex wake asymmetry over a substantial portion of the *nose* of the aircraft, the resulting smooth variation of nose side force with tip roll angle would translate into a smooth variation of aircraft yawing moment. The result would be a feasible yaw control device for a high-performance aircraft at high angle of attack.

Conclusions

The elliptic cross-section tip studied in these experiments, with cross sections generated by two sixth-degree polynomials such that the tip radius, slope, and curvature matched that of a right circular cone at the point where the polynomial became tangent to a cone generator, is effective in varying the vortex wake geometry of a right circular cone at large angle of attack. The measured side force coefficient varies smoothly with tip roll angle for the two lowest angles of attack studied and exhibits square-wave and more undesirable variations for the larger angles of attack studied. The square-wave and peak, reduction-in-magnitude, and change-in-sign variations are caused by vortex breakaway, which allows vortex crossover to occur. It is this vortex breakaway that limits the ability of a variation in tip geometry to control the vortex wake asymmetry. Ahead of vortex breakaway, the elliptic cross-section tip yields smooth variations of vortex wake asymmetry with tip roll angle, indicating that the tip would possibly be a feasible control device for high-performance fighter aircraft at high angle of attack.

Acknowledgments

This work was supported in part by the Office of Naval Research Grant N00014-90-J-1305, Modification P00003. The authors are indebted to a reviewer for recalling to their attention two important background references.

References

[1]Ericsson, L. E., and Reding, J. P., "Vortex-Induced Asymmetric Loads in 2-D and 3-D Flows," AIAA Paper 80-0181, Jan. 1980.

[2]Ericsson, L. E., and Reding, J. P., "Asymmetric Vortex Shedding from Bodies of Revolution," *Tactical Missile Aerodynamics*, edited by M. J. Hemsch and J. N. Nielsen, Vol. 104, Progress in Astronautics and Aeronautics, AIAA, New York, 1986, pp. 243–296.

[3]Hunt, B. L., "Asymmetric Vortex Forces and Wakes on Slender Bodies," AIAA Paper 82-1336, Aug. 1982.

[4]Rao, D. M., Moskovitz, C., and Murri, D. G., "Forebody Vortex Management for Yaw Control at High Angles of Attack," *Journal of Aircraft*, Vol. 24, No. 4, 1987, pp. 248–254.

[5]Guyton, R. W., Osborn, R. F., and LeMay, S. P., "Forebody Vortex Control Aeromechanics," *Manoeuvring Aerodynamics*, AGARD CP-497, Paper 16, May 1991.

[6]Malcolm, G. N., and Ng, T. T., "Aerodynamic Control of Fighter Aircraft by Manipulation of Forebody Vortices," *Manoeuvring Aerodynamics*, AGARD CP-497, Paper 15, May 1991.

[7]Williams, D. R., and Bernhardt, J. E., "The Effect of Reynolds Number on Vortex Asymmetry About Slender Bodies," *Physics of Fluids A*, Vol. 5, No. 2, 1993, pp. 291–293.

[8]Moskovitz, C. A., "An Experimental Investigation of the Physical Mechanisms Controlling the Asymmetric Flow Past Slender Bodies at Large Angles of Attack," Ph.D. Thesis, North Carolina State Univ., Dept. of Mechanical and Aerospace Engineering, Raleigh, NC, 1989.

[9]Moskovitz, C. A., Hall, R. M., and DeJarnette, F. R., "Effects of Nose Bluntness, Roughness, and Surface Perturbations on the Asymmetric Flow Past Slender Bodies at Large Angles of Attack," AIAA Paper 89-2236-CP, July 1989.

[10]Zilliac, G. G., Degani, D., and Tobak, M., "Asymmetric Vortices on a Slender Body of Revolution," *AIAA Journal*, Vol. 29, No. 5, 1991, pp. 667–675.

[11]Skow, A. M., and Erickson, G. E., "Modern Fighter Aircraft Design for High-Angle-of-Attack Maneuvering," *High Angle of Attack Aerodynamics*, AGARD LS-121, Paper 4, March 1982.

[12]Edwards, O. R., "Northrop F-5F Shark Nose Development," NASA CR-158936, Oct. 1978.

[13]Moskovitz, C. A., Hall, R. M., and DeJarnette, F. R., "New Device for Controlling Asymmetric Flowfields on Forebodies at Large Alpha," *Journal of Aircraft*, Vol. 28, No. 7, 1991, pp. 456–462.

[14]Bridges, D. H., "Tip Effects on the Vortex Wake of an Axisymmetric Body at Angle of Attack," Ph.D. Thesis, California Inst. of Technology, Dept. of Aeronautics, Pasadena, CA, 1993.

[15]Bridges, D. H., and Hornung, H. G., "Effects of Tip Reynolds Number and Tip Asymmetry on Vortex Wakes of Axisymmetric Bodies at Various Angles of Attack," AIAA Paper 92-0406, Jan. 1992.

[16]Ward, T., "The Hydrodynamics Laboratory at the California Institute of Technology—1976," Transactions of the ASME, *Journal of Fluids Engineering*, Vol. 98, No. 6, Transactions of the ASME, 1976, pp. 740–748.

[17]Lamont, P. J., "Pressures Around an Inclined Ogive Cylinder with Laminar, Transitional, or Turbulent Separation," *AIAA Journal*, Vol. 20, No. 11, 1980, pp. 1492–1499.

[18]Thomson, K. D., and Morrison, D. F., "The Spacing, Position, and Strength of Vortices in the Wake of Slender Cylindrical Bodies at Incidence," *Journal of Fluid Mechanics*, Vol. 50, Pt. 4, 1971, pp. 751–783.

[19]Wardlaw, A. B., Jr., and Yanta, W. J., "The Flow Field About, and Forces on Slender Bodies at High Angles of Attack," AIAA Paper 80-0184, Jan. 1980.

[20]Milne-Thomson, L. M., *Theoretical Hydrodynamics*, 5th ed., MacMillan, New York, 1968, p. 369.

[21]Ward, K. C., and Katz, J., "Development of Flow Structures in the Lee of an Inclined Body of Revolution," *Journal of Aircraft*, Vol. 26, No. 3, 1989, pp. 198–206.

[22]Kompenhans, J., and Hartmann, K., "Flow Visualization on an Ogive-Nosed Circular Cylinder Body at High Incidence by Means of the Laser Light Sheet Method," European Space Agency, Paris, ESA TT 1066, Sept. 1987 (translation of "Stroemungssichtbarmachung an einem hochangestellten Ogigkreiszylinderrumpf mit Hilfe der Laser-Lichtschnittmethode," DFVLR-FB-86-45, Nov. 1986).

[23]Degani, D., and Tobak, M., "Experimental Study of Controlled Tip Disturbance Effect on Flow Asymmetry," *Physics of Fluids A*, Vol. 4, No. 12, 1992, pp. 2825–2832.

[24]Keener, E. R., and Chapman, G. T., "Similarity in Vortex Asymmetries over Slender Bodies and Wings," *AIAA Journal*, Vol. 15, No. 9, 1977, pp. 1370–1372.

[25]Ericsson, L. E., "Sources of high alpha vortex asymmetry at zero sideslip," *Journal of Aircraft*, Vol. 29, No. 6, 1992, pp. 1086–1090.

[26]Bernhardt, J., and Williams, D., "The Effect of Reynolds Number on Control of Forebody Asymmetry by Suction and Bleed," AIAA Paper 93-3265, July 1993.

[27]Keener, E. R., "Flow Separation Patterns on Symmetric Forebodies," NASA TM 86016, Jan. 1986.

[28]Chambers, J. R., Anglin, E. L., and Bowman, J. S., Jr., "Effects of a Pointed Nose on Spin Characteristics of a Fighter Airplane Model Including Correlation with Theoretical Calculations," NASA TN D-5921, Sept. 1970.

[29]Keener, E. R., and Chapman, G. T., "Onset of Aerodynamic Side Forces at Zero Sideslip on Symmetric Forebodies at High Angles of Attack," AIAA Paper 74-770, Aug. 1974.